PHOTONS FROM THE NUCLEAR COULOMB FIELD AND FROM INTERACTIONS OF CONSTITUENTS*,**

By T. Ferbel***

University of Rochester, Rochester, N.Y.14627, USA

(Received August 26, 1981)

In these lectures I will describe our group's recent experiments performed in the Meson Area of Fermilab. I will begin with a discussion of the theoretical motivation for the investigation of the interactions of mesons in the nuclear Coulomb field, describe the apparatus used in the studies and the results obtained thus far, then I will proceed to a brief description of the physics of direct-photon production in hadronic reactions and, finally, to our tests of the feasibility of using a liquid-argon detector for studying such processes at Tevatron energies.

PACS numbers: 13.85.-t

1. Introduction — electromagnetic transitions

Hadron-nuclear collisions have received a grat deal of attention during this past decade [1]. Although, in the main, interest has focused on incoherent reactions, particularly on the question of the time-development of hadronic processes, there has also been substantial activity in the area of inelastic coherent production. Coherent reactions have been used to study diffractive processes, interactions in the nuclear Coulomb field, and isoscalar-exchange mechanisms. In what follows I will provide the motivation for investigating coherent inelastic interactions of mesons in the nuclear Coulomb field in the range of Fermilab-SPS energies.

The specific diagram I have in mind is the Primakoff process [2] indicated in Fig. 1, in which a hadron (h) interacts via photon exchange with a nucleus of charge Z and nucleon number A, producing a hadronic system (or particle) h*, while leaving the recoiling

---

* Presented at the XXI Cracow School of Theoretical Physics, Paszkówka, May 29–June 9, 1981.

** Research supported by the United States Department of Energy.

*** Visitor at CERN, Geneva, Switzerland.

nucleus in its ground state [3]. If the cross-section for such an electromagnetic transition can be extracted from the data, then, employing the Primakoff formalism, it can be used to determine the radiative width ($\Gamma_{h^* h\gamma}$) for the decay $h^* \to h\gamma$, or to study $h\gamma$ elastic Compton scattering (for the case of h^* decaying into h-γ), or to measure in an unambiguous way h-π scattering phase shifts (if h^* decays eventually into an h-π system).

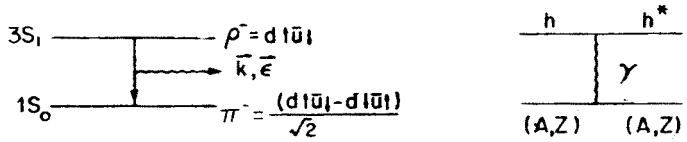

Fig. 1. At the right is the diagram for the Primakoff production of an excited hadron state (h^*) in the Coulomb field of a nucleus of charge Z. At the left is an energy-level diagram of the quark-antiquark states involved in the $\rho^- \to \pi^-\gamma$ transition

In addition, and on a more speculative note, because meson-photon incident channels have not been investigated in great detail in the past, particularly for masses above 1 GeV, these reactions could therefore provide surprises, such as the production of new families of resonances that might be forbidden to decay hadronically but could be observed electromagnetic channels.

2. *SU(3) — quarkology*

The radiative decay $\rho^- \to \pi^-\gamma$ can be regarded in the simple quark model as a magnetic-dipole transition between a $^3S_1$ and a $^1S_0$ level of a quark-antiquark system. Figure 1 displays the specific quark states relevant to the process. In the long-wavelength approximation, the M-1 operator for any such vector meson-pseudoscalar decay transition can be written as [4]:

$$H \simeq \sum_j \mu_j \vec{\sigma}_j \cdot (\vec{k} \times \vec{\varepsilon}), \tag{1}$$

where the summation is over the quarks with magnetic moments μ_j; $\vec{\varepsilon}$ and $\vec{k}$ are, respectively, the polarization and momentum vector of the emitted photon; $\vec{\sigma}_j$ are the Pauli spin matrices.

The radiative width for the $V \to P\gamma$ decay can be written (for non-relativistic quarks) in terms of H as follows:

$$\Gamma_{VP\gamma} \simeq \frac{4k}{3}\left(\frac{E_P}{M_V}\right) \sum_{\langle i\rangle,f} |\langle P_f|H|V_i\rangle|^2, \tag{2}$$

where M_V is the mass of the vector meson, and E_P is the energy of the pseudoscalar in the rest frame of V; the sum is over all final states and an average over initial states.

Ambiguities inherent in the derivation of Eq. (2) make the absolute predictions for radiative widths somewhat suspect [5]. Nevertheless, when the same kind of quarks are

involved, the ratios of predicted widths would be expected to be far more reliable. The calculations should be particularly trustworthy in the case of a comparison between $\Gamma(\omega^0 \to \pi^0\gamma)$ and $\Gamma(\rho \to \pi\gamma)$ because the kinematics in both decays are essentially the same and, for the case of ideal mixing, the ω^0 meson can be described by an equal superposition of $u\bar{u}$ and $d\bar{d}$ quarks. Using Eq. (2), the ratio of $\Gamma_{\varrho\pi\gamma}/\Gamma_{\omega\pi\gamma}$ is expected to be 85 keV/780 keV, or ~ 0.11. (The same result for the ratio can also be obtained simply from SU(3) Clebsch-Gordan coefficients, assuming that the photon is the U = 0 member of the vector-meson octet.) The experimentally determined ratio, prior to our measurements, was 0.045 ± 0.013 — a result quite inconsistent with expectation. Because the experimental value of $\Gamma_{\omega\pi\gamma}$ agreed reasonably well with the theoretical prediction, it was natural (particularly for theorists!) to view the previous value [6] of $\Gamma_{\varrho\pi\gamma}$ with some suspicion.

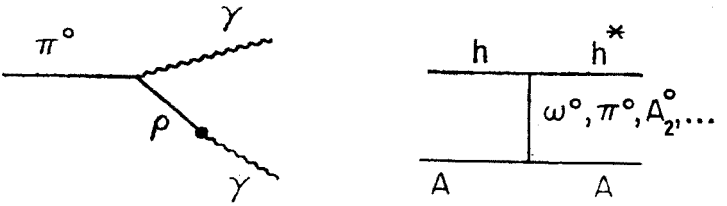

Fig. 2. The diagram used in the calculation of $\Gamma_{\varrho\pi\gamma}$ via the vector meson dominance hypothesis is shown at the left. Strong-exchange contributions to coherent production of h*, on a nucleus of nucleon number A, are given at right

An independent calculation [5] of $\Gamma_{\varrho\pi\gamma}$, based on the vector-dominance hypothesis in $\pi^0 \to \gamma\gamma$ decay (see Fig. 2), also suggested that $\Gamma_{\varrho\pi\gamma}$ should be ~ 70 keV rather than the old 35 ± 10 keV value [6]. This theoretical difficulty prompted our attempt for a second-generation measurement of the $\rho^- \to \pi^-\gamma$ decay.

3. *Primakoff process*

At first glance, one might be tempted to try to measure the $\rho^- \to \pi^-\gamma$ branching width through a comparison of this decay mode with the more favoured $\rho^- \to \pi^-\pi^0$. Unfortunately, the ratio $\Gamma_{\varrho\pi\gamma}/\Gamma_{\varrho\pi\pi}$ is expected to be $\lesssim 10^{-3}$; consequently, $\rho^- \to \pi^-\pi^0 \to \pi^-\gamma\gamma$ decays in which one of the photons escapes detection (and this occurs, typically, at the $\gtrsim 10^{-2}$ level) can feed through to the $\rho^- \to \pi^-\gamma$ candidates and cause insurmountable background problems. (Comparing $\rho^0 \to \pi^+\pi^-$ with $\rho^0 \to \pi^0\gamma$ will not help because of the large $\pi^0\pi^0$ backgrounds that usually prevail in any suitable ρ^0-production reaction; for example, the cross-section for $\pi^+p \to \Delta(1232)^{++}\rho^0$ is comparable to $\pi^+p \to \Delta(1232)^{++}\pi^0\pi^0$, where the two π^0's are either in the $I = 0$ or 2 state.)

Another possibility for measuring $\Gamma_{\varrho\pi\gamma}$ is, for example, through the extraction of the strength of the $\rho\pi\gamma$ vertex in ρ^+ photoproduction on a hydrogen target. This involves the isolation of the π-exchange contribution to the cross-section and delicate, but ultimately unreliable, extrapolations of the coupling to the pion pole.

As in the previous experiment [6], we decided to utilize the nuclear Coulomb field as a source of photons to measure the inverse process $\pi^-\gamma \to \rho^-$. The cross-section for the production of any object h* in the Coulomb field of a nucleus can be written as [2]:

$$\frac{d\sigma_c}{dtdM^{*2}} \equiv |F_c|^2 = \frac{Z^2\alpha}{\pi} \frac{\sigma_\gamma(M^*)}{M^{*2}-M^2} \frac{t-t_0}{t^2} |F_{EM}(t)|^2, \tag{3}$$

where α is the fine-structure constant, M^* is the mass of h* and M the mass of h, $\sigma_\gamma(M^*)$ is the cross-section for the reaction $\gamma h \to h^*$ at $\sqrt{s} = M^*$ for γh, t_0 is the square of the minimum momentum transfer required to produce M^*, and $F_{EM}(t)$ is the electromagnetic form factor of the nucleus. When h* is a resonance that decays into some particular channel, e.g. $h^* \to h\pi$, then we can write for $\sigma_\gamma(M^*)$, the cross-section for $h\gamma \to h\pi$, as follows:

$$\sigma_\gamma(M^*) = \frac{2\pi^2}{q^2} \frac{(2J^*+1)}{(2J+1)} \frac{M_0^2\Gamma_\gamma(M^*)\Gamma_\pi(M^*)}{(M^{*2}-M_0^2)^2+M_0^2\Gamma_T^2(M^*)}, \tag{4}$$

where J and J^* are the spins of h and h*, M_0 is the mass of h* on resonance; Γ_T, Γ_γ, and Γ_π are the mass-dependent total, radiative ($h^* \to h\gamma$) and partial ($h^* \to h\pi$) decay widths of h*. The cross-section for producing h* is therefore proportional to Γ_γ. It is also proportional to Z^2 and has the characteristic t^{-2} behaviour of the photon propagator. The cross-section must vanish at 0° ($t = t_0$) and it peaks at $2t_0$. For $M^* \sim 1$ GeV and for incident momenta of ~ 200 GeV/c, t_0 is $\sim 5\times10^{-6}$ GeV^2, which corresponds to impact parameters of ~ 50 fm. Because the cross-section in Eq. (3) is steeply peaked at such small t values, the calculation is insensitive to the detailed form of $F_{EM}(t)$.

As the incident momentum (p) increases, the value of t_0, at fixed M^*, decreases as p^{-2}. This opens up a new region of phase space for the Primakoff process and the total cross-section therefore increases with energy; although asymptotically this growth is only logarithmic in p, for high values of M^* (or for small values of p) the p-dependence is far stronger. Background contributions that involve particle exchanges (see Fig. 2) fall rapidly with energy and, consequently, the measurement of a radiative width via photon exchange is greatly facilitated by performing such an experiment at high energies where electromagnetic production dominates over any strong-exchange contributions.

4. Interference from strong production

The cross-section for coherent production of h* through isoscalar exchange (e.g. ω^0 in Fig. 2) can be parametrized as follows [2]:

$$\frac{d\sigma}{dt} = |F_s|^2 = A^2(t-t_0)C_s|F_H(t)|^2, \tag{5}$$

where C_s, determined by production on a nucleon target, contains the energy dependence ($\sim p^{-1}$), and $|F_H(t)|^2$ is the nuclear form factor. Because distances of the order of several fm are involved, the calculations based on Eq. (5) are far more sensitive to details of the nuclear-shape parameters than is the case for Eq. (3).

For coherent ρ^- production, either through γ-exchange and through ω-exchange, the ρ^- is produced with helicity projections of ± 1 along the exchange direction (Gottfried-Jackson frame). Thus, when the ρ^- decays into a $\pi^-\pi^0$ system, the angular distribution will be of a $\sin^2\theta \cdot \sin^2\phi$ form. Consequently, the electromagnetic and the strong contributions to ρ^- production have to be extracted through an analysis of the dependence of the data on t, A and, to a lesser extent, on p. Our procedure is to integrate the data (and the theoretical expressions) over a certain range of M^* values and then fit the data to the following theoretical expression:

$$\frac{d\sigma}{dt} = |F_c + F_s \exp(i\phi)|^2, \tag{6}$$

where F_c and F_s are the electromagnetic and strong amplitudes (integrated over some finite mass interval), and ϕ is the phase of the strong amplitude relative to the Coulomb term. (The Coulomb phase is included in F_c.) Because of the uncertainty in the formula we employ for strong exchanges, we allow C_s to vary freely, but check that it is reasonably consistent with what might be expected from production on hydrogen. Consequently, in our fits we have three parameters: C_s, ϕ, and Γ_γ. (When the fits warrant it and backgrounds are large enough, we introduce an additional incoherent term of the form $D \exp Et$ into Eq. (6).) The fits to the data are very sensitive to the experimental resolution, and the theoretical expressions for F_s and F_c are therefore corrected for resolution smearing in the comparison with data.

At the energies of our experiment we are insensitive to strong-exchange contributions that involve $I \neq 0$. These cross-sections fall more rapidly with increasing energy and scale as the neutron-proton difference in a nucleus [7].

5. *The experimental set-up for E272*

Experiment E272 was performed in the M-1 beam of Fermilab. The first run was taken in a negative beam at two energies: 156 GeV/c and 260 GeV/c [8]. The set-up is illustrated schematically in Fig. 3. The basic elements consisted of: *i*) A target box that was surrounded

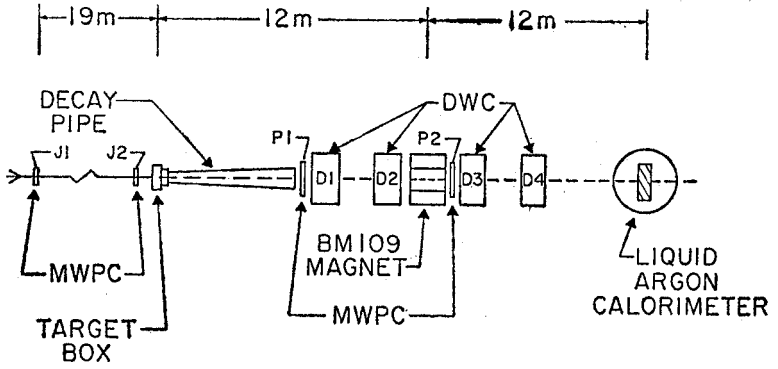

Fig. 3. Experimental layout for E272

with lead/scintillator-sandwich veto counters, used to suppress interactions that involved nuclear break-up or multiple-particle production. *ii*) A drift wire chamber (DWC) system (D1, D2, D3, and D4) used to measure charged-particle trajectories. *iii*) Multiwire proportional chamber (MWPC) planes, used for beam tagging (J1 and J2) and for triggering purposes (P1 and P2). *iv*) A liquid-argon calorimeter (LAC), used for measuring the deposition of electromagnetic energy.

The evacuated decay region downstream of the target was used for obtaining a clean sample of beam K^- decays that served to normalize our cross-sections and to check our experimental resolution.

The positions of various scintillation tirgger and veto counters in the experiment are shown in Fig. 4. All the A_i and V_{ij} were used in veto. The AM elements formed the limiting

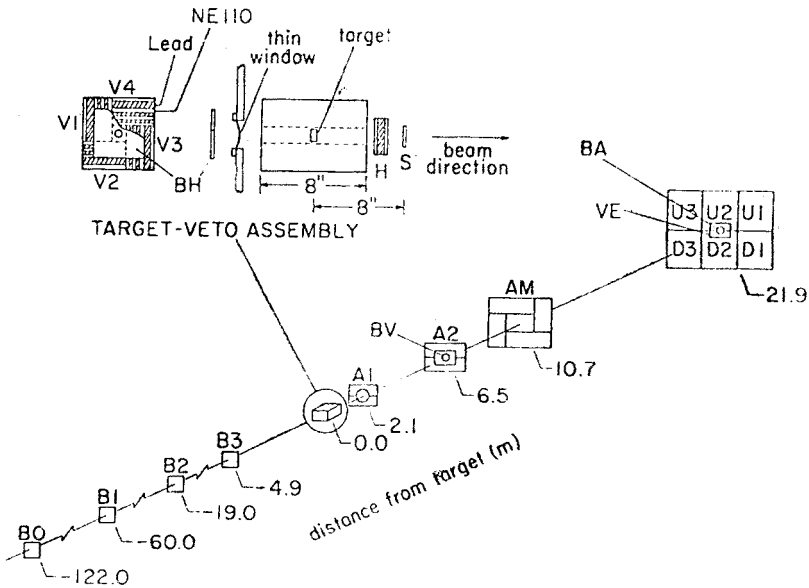

Fig. 4. Scintillation counters used in E272

aperture on the front face of the analysing magnet (BM109). In the ρ^- type of trigger (one minimally ionizing particle exiting the target, as inferred via a discriminator setting on the output pulse of the 1.6 mm thick S-counter) a small veto counter (BA) was used to veto events that had a charged track in the beam region at the position of the LAC. This eliminated from consideration most of the non-interacting beam tracks (which, clearly, satisfy all the veto requirements) and small-angle elastic scatters. The BH counter was a scintillator that had a hole the size of the beam spot (~ 1 cm); this was used to veto incident tracks in the beam-halo region. The B_i counters, in conjunction with BH, were used to define acceptable beam. Three Čerenkov counters located in the beam between B0 and B2 enabled us to distinguish incident π^-, K^-, and $\bar{p}$ components.

Figure 5 shows the geometry of the LAC construction. Once all cells were assembled, the detector was immersed into a vacuum-walled dewar, filled with liquid argon, and kept cool through a liquid nitrogen heat-exchanging loop located at the top of the dewar (above the level of the liquid argon). The LAC was divided into equal front and back halves. All the x channels (and y channels) in front and in back, that were at the same distance

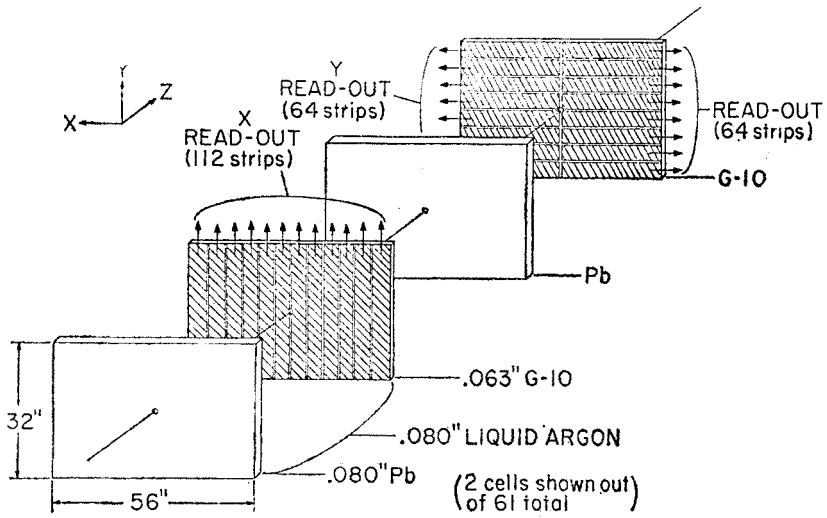

Fig. 5. Sketch of x-y read-out boards and assembly of LAC

from the beam axis, were ganged together and read out on low impedance cables through a cover on the top of the dewar. Here the signals were amplified and eventually digitized using a novel sample and hold system [9].

The lead plates on the LAC were set typically to about -1500 V relative to the copper strips. Under normal conditions, an electron or photon that entered the LAC initiated an electromagnetic cascade in the lead that produced a large number of electrons. These electrons then ionized the argon atoms, causing current to flow between the lead plates and the copper strips near the position of the cascade. This current pulse was detected and analysed using the read-out circuitry.

A hole was drilled through the lead plates and the G-10 boards in the region of the beam to minimize interactions of beam particles within the LAC. Nevertheless, a sufficiently large number of hadrons interacted in the LAC so that special measures had to be taken to reduce the trigger rate for ρ^--like events.

6. *The* ρ^- *trigger*

A ρ^- trigger could in principle be defined through a beam-track requirement, an S counter minimum-ionizing signal and an energy deposition in the LAC. Unfortunately, $\gtrsim 10^{-2}$ of all beam tracks (all outside of the BH-veto region) would pass such weak constraints.

This is because even though the LAC had a beam hole, just outside of this hole any incident hadrons could interact ($\sim$ 0.7 interaction lengths of material) and produce π^0's that could deposit substantial energy in the LAC. Thus, without additional protection, elastically scattered beam tracks could often simulate ρ^- triggers, and because the ratio of the ρ^- cross-section to elastic scattering on a copper target, for example, is $\lesssim 10^{-3}$, even a minuscule feedthrough of elastic scatters at the trigger stage could have greatly compromised the experiment. This is because experiments tend to be limited by the number of events that can be written on tape — in our case this was about 40/s. If our trigger rate were limited by elastic scatters to$\sim 10^{-2}$ of the beam rate, then we would have been able to utilize only $\sim 4\times 10^3$ beam/s for producing ρ^- events, instead of the $\sim 4\times 10^5$ beam/s that we eventually used, after we tightened up the trigger requirements.

To tighten requirements on the ρ^- trigger we utilized the fact that, for real electromagnetically-produced ρ^- events, the π^- and π^0 decay products are emitted in opposite vertical directions relative to the beam line. Thus, electromagnetic energy in the upper part of the LAC must be correlated with the presence of a charged particle in the lower part of the LAC and vice versa. By requiring in the trigger that the up/down scintillation counters (U_i/D_i at front of the LAC) be correlated with energy in this particular way greatly suppressed the major background from events in which a lone charged hadron interacted in the LAC, simulating the presence of an electromagnetic shower.

Two other precautions were taken to further reduce background-ρ^- triggers. First, the P1 and P2 chambers were interrogated [10] to check that the charged-track multiplicity in front and downstream of the magnet was consistent with that for a ρ^- event. Second, a matrix was set up between wires in J1, J2, and P1 to ascertain that the triggers were due to interactions in the target. That is, using the slope of the beam trajectory obtained from J1 and J2, the track position was extrapolated to wires in the P1 chamber. If these P1 wires had signals, it was assumed that the beam track interacted somewhere downstream of the target and the event could therefore be rejected at the trigger stage. Using all the above criteria, the ρ^- trigger rate was eventually reduced to $\sim 10^{-5}$ of the beam, essentially without biasing the true ρ^- signal.

7. Studies of K^- decays

Decays of the type $K^- \to \pi^-\pi^0$ or $K^- \to \pi^0 e^-\bar{\nu}$ have the same topology as the $\rho^- \to \pi^-\pi^0$ events. These decays were collected simultaneously with the normal ρ^- triggers and were used to fine-tune the parameters in the Monte-Carlo acceptance program for the experiment.

Figure 6 illustrates how the resolution in t degrades with target material and with increasing beam momentum. The steepest distribution is for $K_{\pi 2}$ decays that occured in the vacuum pipe when there was no target in the target box. If our resolution were perfect, then all the events would be located at $t = 0$. But because of measuring error the sum of the π^- and π^0 vector momenta is not equal to that measured for the incident K^-. When a Pb target ($\sim$ 0.2 radiation length of material) is introduced into the target box the incident K^- undergoes multiple-Coulomb scattering which smears the measurement of the

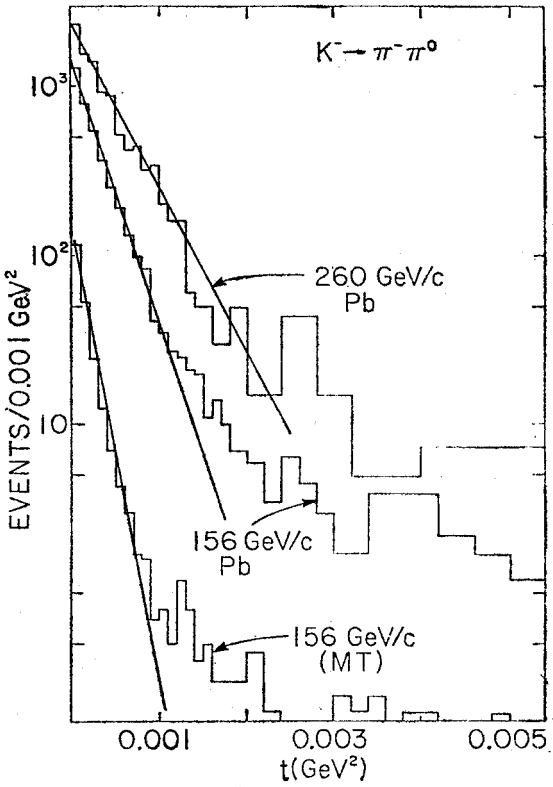

Fig. 6. The t distributions for $K_{2\pi}$ decays under different experimental conditions

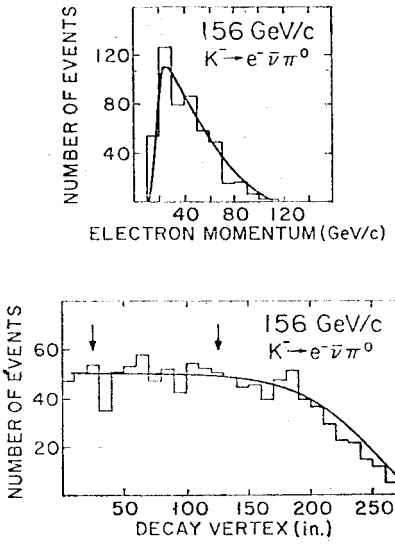

Fig. 7. Comparison of K_{e3} decays with expectations from the Monte Carlo (smooth curves)

incident angle, thereby worsening the resolution in t (given essentially by $p \cdot \delta\theta$). When, in addition, the beam momentum is increased, the t resolution is observed to broaden further. The tails to the simple exponential fall-offs in Fig. 6 are mainly due to small backgrounds from $K_{\mu 3}$ or $K_{\pi 3}$ decays of the K^-.

Figure 7 displays the electron momentum distribution and the location of the decay point in the vacuum pipe downstream of the target for the K_{e3} events. The smooth curves are the expectations from the Monte Carlo program, which was based mainly on studies of the $K_{\pi 2}$ decays. The agreement is clearly quite good. Other detailed studies of this kind have given us confidence that we understand the resolution and acceptance of the entire spectrometer.

8. Check of the Primakoff formalism

To check the validity of our analysis and of the Primakoff formalism, we used data available for the reaction $\gamma p \to p\pi^0$ near the region of the $\Delta(1232)$ [11], in conjunction with Eq. (3), to predict the rate for $\Delta(1232)$ production for proton interactions in the

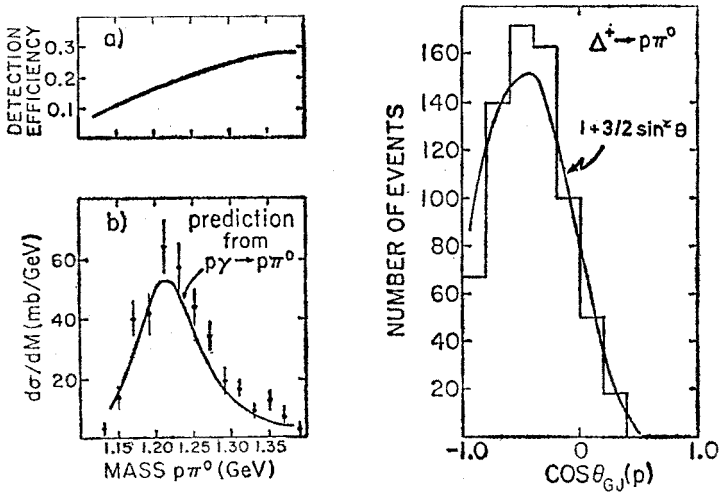

Fig. 8. Comparison of the T(1232)$^+$ signal observed on a Pb target with expectations from Primakoff production

nuclear Coulomb field. Because the $\bar{p}$ flux in the negative beam was too small, we therefore ran a short time at 156 GeV/c in a positive beam. These data were used to check that the cross-section for the reaction $p + Pb \to p\pi^0 + Pb$ agreed with expectations.

Figure 8 displays the data for $p\pi^0$ production on Pb at small t, where Coulomb production should dominate. The overall acceptance is rather poor (primarily because the π^0's are of low momentum and their decay products miss the LAC). The observed cross-section as a function of $p\pi^0$ mass is in agreement with the prediction (smooth curve), particularly at low masses. At higher masses, diffractive N*(1400) production becomes

important and the data consequently deviate from the prediction that is based solely on Eq. (3). The angular decay distribution of the proton in the $\Delta(1232)$ rest frame (Gottfried-Jackson) is in agreement with the $1+{}^3/_2 \sin^2\theta$ form expected from the interaction of a transversely polarized photon with a proton in the $J = {}^3/_2$ state.

Hence, to $\sim 20\%$ accuracy, limited by a combination of statistics, uncertainty in resolution, and uncertainty in the cross-section for $\gamma p \to p\pi^0$, the predictions are in agreement with our observations for $\Delta(1232)$ production in the nuclear Coulomb field.

9. *Radiative width of the* ρ^-

Distributions in the reconstructed vertex positions for 156 GeV/c and 260 GeV/c data for the reaction:

$$\pi^- \mathrm{Pb} \to \pi^- \pi^0 \mathrm{Pb} \tag{7}$$

are shown in Fig. 9. The data are completely consistent with the smooth curves, which represent what is expected from the resolution of the spectrometer. (The target thickness is only ~ 1.5 mm: hence, the widths of these distributions are entirely due to experimental resolution).

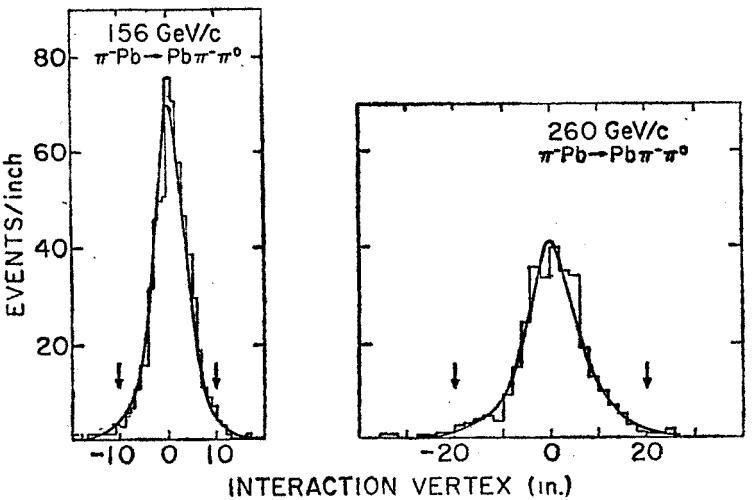

Fig. 9. Distribution in the reconstructed interaction vertexes near the target for reaction (7). The smooth curves are expectations based on Monte Carlo calculations

Distributions in the total energy of $\pi^-\pi^0$ systems for candidate events for reaction (7), and for similar data on a carbon target, are shown in Fig. 10. The cross-hatched regions correspond to events with $t < 0.002\ \mathrm{GeV}^2$. The low-energy tail, particularly evident in the carbon sample, stems from A_1^- background, in which the coherently-produced A_1^- events decay into $\pi^-\pi^0\pi^0$ systems and one of the π^0's either misses the LAC or has too little energy to be properly reconstructed. This sort of background provides artificial ρ^-

events that have large apparent t-values. The arrows in the figure indicate the cuts on the range of energies used for defining acceptable events. (The widths of the peaks are due partially to experimental resolution and partially to the inherent ~1% spreads in the beam momenta.)

The uncorrected mass spectra for $\pi^-\pi^0$ systems produced on several nuclear targets are shown in Fig. 11. The data appear to be dominated by the ρ^- peak. The decay angular

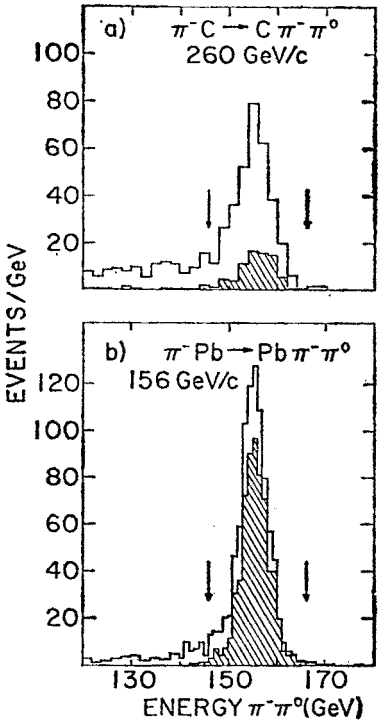

Fig. 10

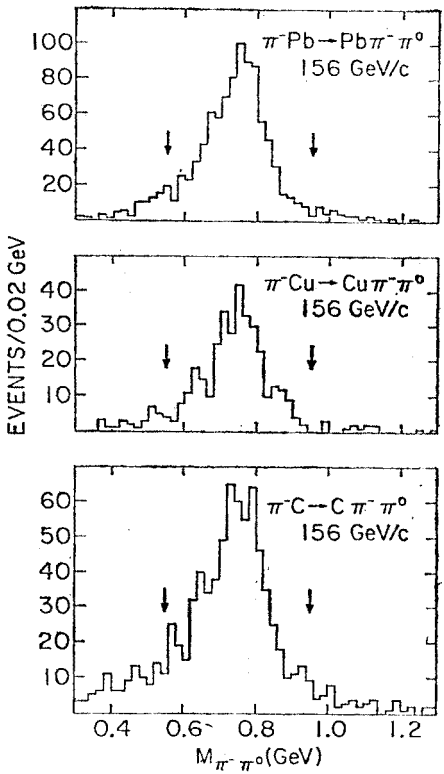

Fig. 11

Fig. 10. Energy of $\pi^-\pi^0$ systems produced in reaction (7) that have vertexes within the arrow-bounds shown in Fig. 9. The cross-hatched regions are for t 0.002 GeV^2

Fig. 11. Mass distributions for $\pi^-\pi^0$ systems produced in reaction (7), that have acceptable vertex and energy bounds

distribution of the ρ^-, for events having $t < 0.002$ GeV^2, where background from A_1^- production is negligible, is consistent with the expected $\sin^2\theta \cdot \sin^2\phi$ form. This is demonstrated in Fig. 12, where the smooth curves represent the $\sin^2\theta$ dependence, corrected for acceptance and resolution. (The ϕ dependence at small t is dominated by the resolution. At larger t, as in carbon, for example, there is a clear indication of a $\sin^2\phi$ behaviour.)

The cross-section for reaction (7) as a function of $\pi^-\pi^0$ mass, corrected for all cuts, resolution and acceptance, is given in Fig. 13 [12]. [The curves on the data represent different

parametrizations of the ρ^- line shape using Eqs. (3) and (4).] Also in Fig. 13, there appear two typical fits of Eq. (6) to the data, integrated over $\pi^-\pi^0$ mass. The cross-sections at small values of t scale essentially as Z^2, while at larger t, where ω^0 exchange becomes more significant, the fits and data develop a weaker A-dependence.

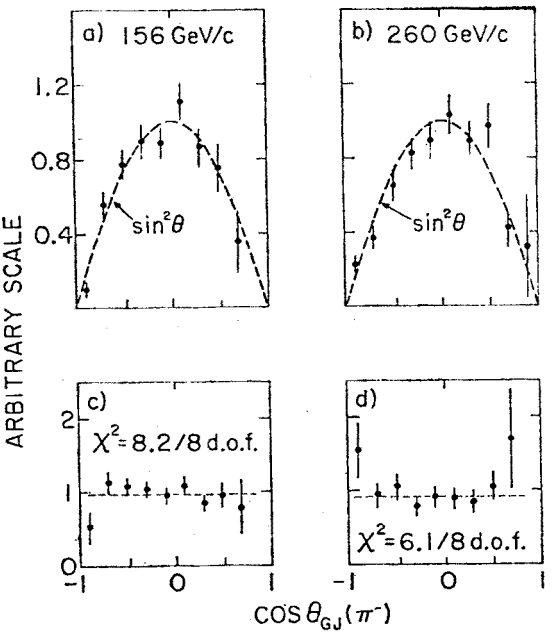

Fig. 12. Angular decays of ρ^- mesons produced on a Pb target at $t < 0.002$ GeV^2. The smooth curves correspond to the expected forms for Coulomb-produced ρ^-, corrected for acceptance and resolution of the equipment. The points in parts c) and d) show the ratio of the acceptance-corrected ρ^- data to the corresponding $K^- \to \pi^-\pi^0$ decays. The values of χ^2 indicate that we do not have θ-dependent losses of $\rho^- \to \pi^-\pi^0$ relative to $K^- \to \pi^-\pi^0$ events. (This is a stringent check of our normalization procedure)

Fits of the kind shown in Fig. 13 were used to extract from the data the three parameters of interest, namely, C_s, ϕ, and $\Gamma_{\varrho\pi\gamma}$ [12]. The target-to-target variations in these parameters were found to be within the systematic and statistical uncertainty of the data. The results from the high-Z targets (Cu and Pb) were essentially insensitive to C_s or to ϕ. The strong-interaction contribution in the carbon data at 156 GeV/c, was significant and, consequently, because of the uncertainties in the parametrization of $F_H(t)$, the result for the width might be regarded with greater suspicion. ($\Gamma_{\varrho\pi\gamma}$ from the carbon sample was, in fact, somewhat lower that for the other nuclei). Our published [12] value of $\Gamma_{\varrho\pi\gamma}$ is 67 ± 7 keV, a result in far better agreement with SU(3) symmetry than the previous measurement.

Although at face value our result for $\Gamma_{\varrho\pi\gamma}$ disagrees strongly with that of the first-generation experiment [6], I believe that this disagreement is not so much in the actual data as in the analysis used in the older work. In that analysis a unique result for $\Gamma_{\varrho\pi\gamma}$

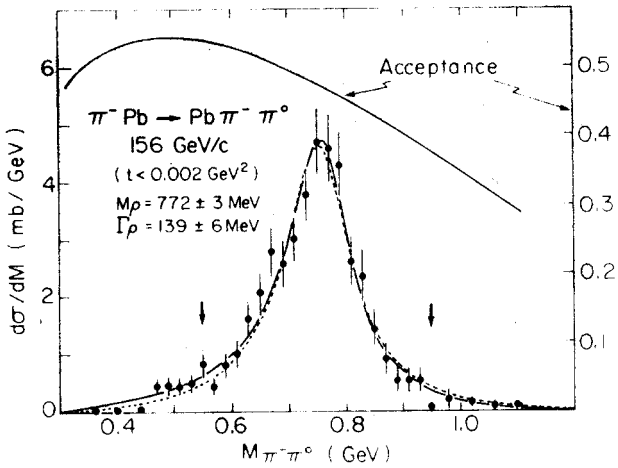

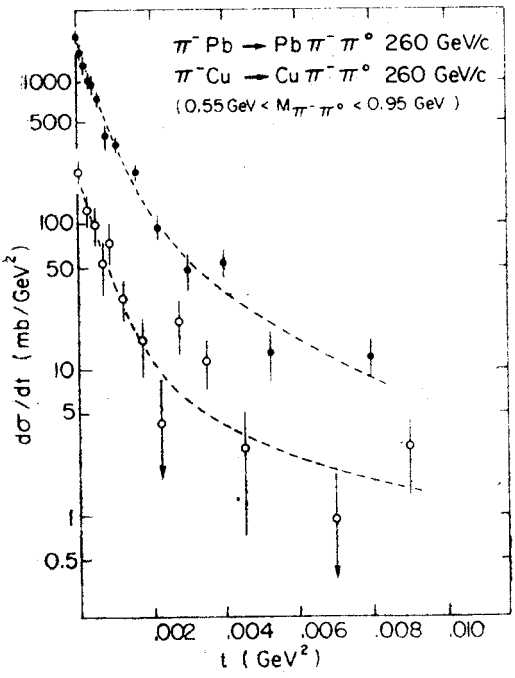

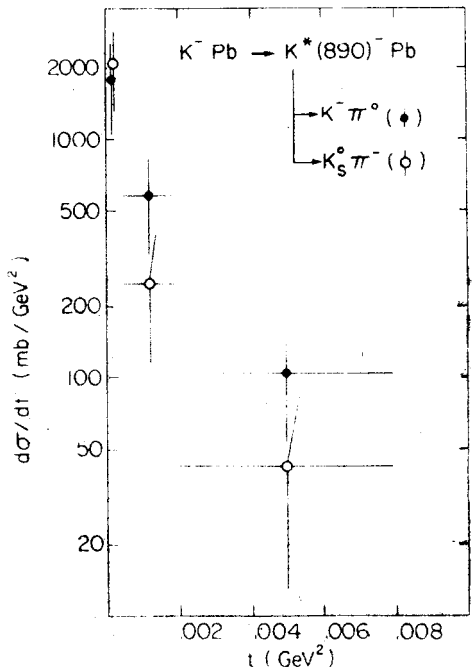

Fig. 13. Mass and t distribution for reaction (7). The smooth curves on the π^- data represent fits used to extract the radiative width of the ρ^-. The t-spectra for $K^*(890)^-$ production on Pb appear in the lower right-hand side of the figure

could be obtained only if C_s were fixed to the same value for all nuclear targets. This is, nominally, an acceptable procedure if the parametrization of the strong-exchange contribution is given solely by the $I = 0$ exchange term of Eq. (5). However, at low energies, $I \neq 0$ exchanges are thought to be important [7], and therefore the coherent ρ^- production cross-section could have an additional contribution proportional to $(A-Z)$. If such an $I = 1$ exchange term exists, then it is improper to fix the parameter C_s to a unique A-independent value. In fact, if this additional constraint is removed in the older data analysis, that experiment can only be used to set limits on $\Gamma_{\varrho\pi\gamma}$ of between 30 ± 10 keV and 80 ± 10 keV [6]. This is, of course, consistent with our measurement. (Unfortunately, the older data are not available for checking the presence of such an $I = 1$ contribution to ρ^- coherent production, and at our energies $I = 1$ exchange is too small to be observed in our experiment.)

10. Radiative width of the K(890)⁻*

The K^- flux in our negative beam was large enough so that we could obtain a first estimate of the radiative decay of the $K^*(890)^-$. Here we had the advantage of having two independent decays of the $K^*(890)$ in the final state, namely, $K^-\pi^0$ (as in the ρ^- measurement, but with the requirement that the beam particle for the trigger was a K^- identified by our Čerenkov counters) and $K^0_s\pi^-$. (The latter decay mode was collected simultaneously with the ρ^- type of triggers. This "V-trigger" had the requirement that one charged track left the target and more than two exited the magnet aperture.) The two sets of data have quite different biases and, consequently, the agreement we obtained for $\Gamma_{K^*-K^-\gamma}$, using these two decay channels [13], is comforting, particularly in light of the poor statistics of our data samples.

Figure 13 shows the t-dependence of the cross-section for $K^*(890)^-$ production on a Pb target at 156 GeV/c. Through a comparison of the individual cross-sections (integrated over mass and t) with the integrated expressions for Eq. (5), a radiative width of 62 ± 14 keV was extracted from data on several nuclear targets. Again, the results were rather insensitive to C_s and ϕ. Our measurement of $\Gamma_{K^*-K^-\gamma}$ is consistent with a previously obtained upper limit for $K^{*+} \to K^+\gamma$ of 80 keV [14].

The absolute value expected for this radiative width, on the basis of quark models, is about 50 keV [15]. The ratio of the previous measurement [16] of the width for $K^*(890)^0 \to K^0\gamma$ to our result: $\Gamma_{K^*-K^-\gamma}/\Gamma_{K^*-K^-\gamma} = 1.2 \pm 0.7$, is inconsistent with the simple SU(3) prediction of four. However, if we assume that symmetry breaking in these decays is similar to that observed in the case of the magnetic moments of baryons [17], then this ratio would equal $[(\mu_d+\mu_s)/(\mu_u+\mu_s)]^2 \simeq 1.6$, which is in agreement with the above ratio of the transition moments.

11. Coherent production of the A_1

Figure 14 displays the cross-section as a function of t for the reaction:

$$\pi^-A \to \pi^-\pi^+\pi^-A. \tag{8}$$

The data are for $(\pi^-\pi^+\pi^-)$ masses below 1.8 GeV, which includes essentially all the events.

(Here, again, the data were collected concurrently with the ρ^- and V samples. The requirement on the A_1 trigger was that three charged tracks had to be detected in the S counter and in the proportional chamber P2.) Instead of plotting the results in terms of t, I have displayed the data as a function of a geometrically scaled t, namely, $\tau = (A/A_{Pb})^{2/3}\, t$, and

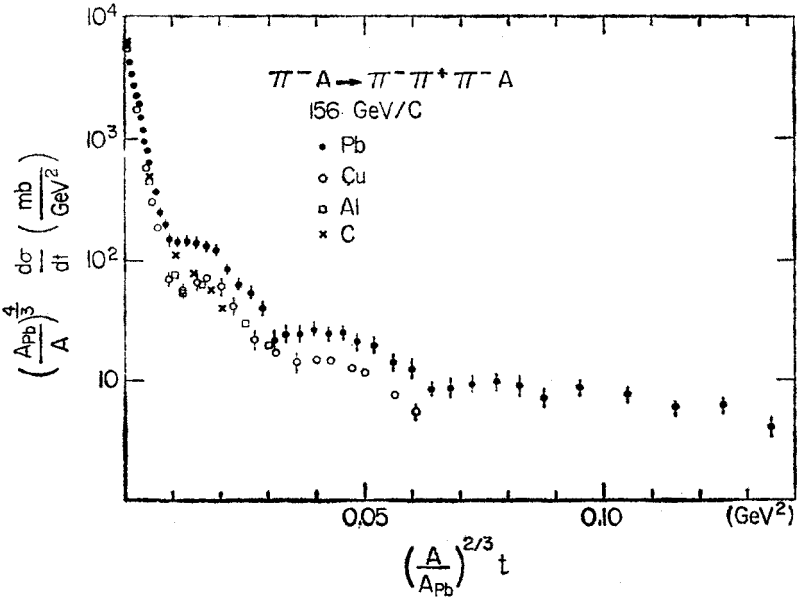

Fig. 14. Distribution in a scaled t-variable for the coherent production of three-pion systems on nuclear targets

have plotted the cross-section multiplied by $(A_{Pb}/A)^{4/3}$. This kind of scaling would be expected if the nucleus could be represented as a black absorbing disk ($d\sigma/dt \sim R^4 \exp(10\, R^2 t)$, with $R \sim A^{1/3}$). To avoid confusion, only several sample points are given for the small-A nuclei at low τ. The dip-bump structure in τ appears to be quite similar for all the nuclei; and although the scaling of the cross-sections for $\tau \lesssim 0.003$ GeV^2 seems quite good, it appears that at larger τ the cross-section for lead exceeds substantially that for the smaller nuclei.

These data are now being analysed for the purpose of extracting the spin-parity content of the $\pi^-\pi^+\pi^-$ system. We have evidence for the Primakoff production in addition to the diffractive production of the A_1^-, but must await the results of this sophisticated analysis prior to making any quantitative statements.

12. Data with positive beam

I have thus far described our progress in analysis of data from a negative-beam run of the experiment. Because the statistics on the K^{*-} width were rather poor, we decided that a second run of the experiment, using a 200 GeV/c positive beam, might be advanta-

geous for improving our results. We changed the magnet polarities and placed a beryllium absorber in the positive-particle beam so as to selectively filter out the protons (and, to a lesser extent, the π^+ component). Figure 15 shows the particle composition of the beam as a function of the beryllium absorber [18]. We ran typically with ~150 cm of Be (placed

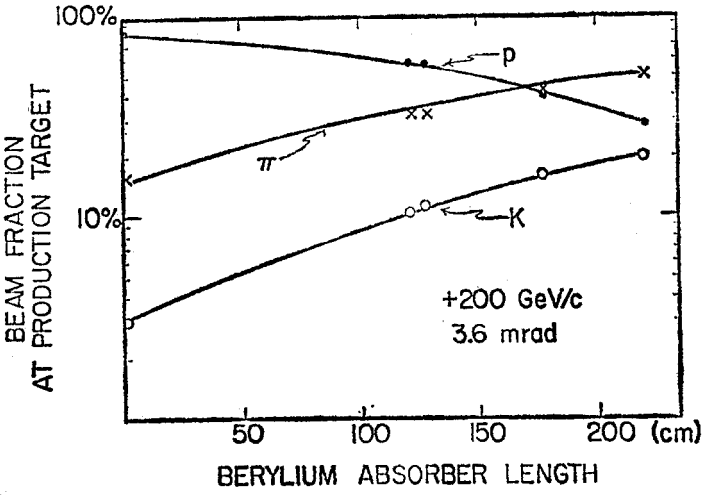

Fig. 15. Particle composition at the target position, as a function of Be absorber upstream in the beam line

at a focus point in the beam so as not to spoil the quality of the optics through the multiple scattering of the surviving particles). This mode of operation, although somewhat wasteful of beam flux, improved our kaon yield by over an order of magnitude relative to that attained in the negative beam.

13. The new data and summary of E272

The run in the positive beam provided us with over a factor of 20 increase in the kaon yield and a factor of 2–3 in the pion yield (the latter, primarily because of improvements, some in the hardware and some in the trigger, achieved during a one year shutdown, the "Mesopause", at the Meson Laboratory). The general quality of the data is best indicated by the $K_s^0\pi^+$ and $K^+\pi^0$ mass distributions for a Pb target (see Fig. 16). In addition to the K*(890) signals there are now also evident sizeable K*(1430) peaks in the data. In fact, the t-distributions of the K*(1430) are exceedingly steep, as expected from electromagnetic roduction; the decay angles (Fig. 16) also suggest that the Primakoff mechanism is dominating. These new data are now being processed through our analysis system and preliminary indications are that $\Gamma_{K^{*+}K^+\gamma}$ will be ~55 keV and $\Gamma_{Q^{+}\pi^+\gamma} \sim$ 70 keV, both consistent with the previous results from our work in the negative beam.

Clear evidence for the electromagnetic production of the B(1235) meson in the new

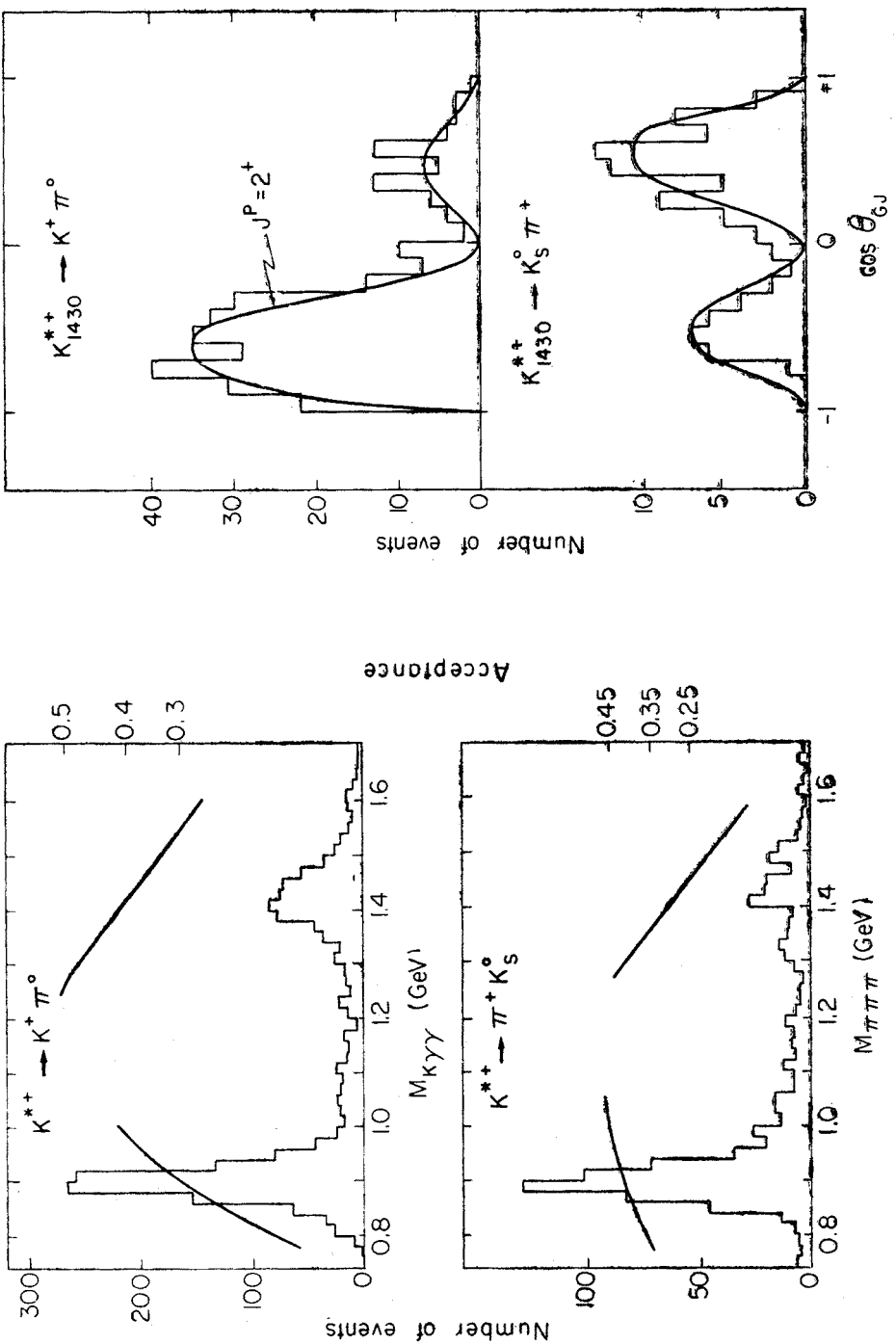

Fig. 16. Mass spectra for coherent production of $K^+\pi^0$ and $K^0_S\pi^+$ systems on a Pb target. The decay angular distributions for events in the K*(1430) region are compared at the right with expectations for the decay of a 2^+ state produced in the nuclear Coulomb field

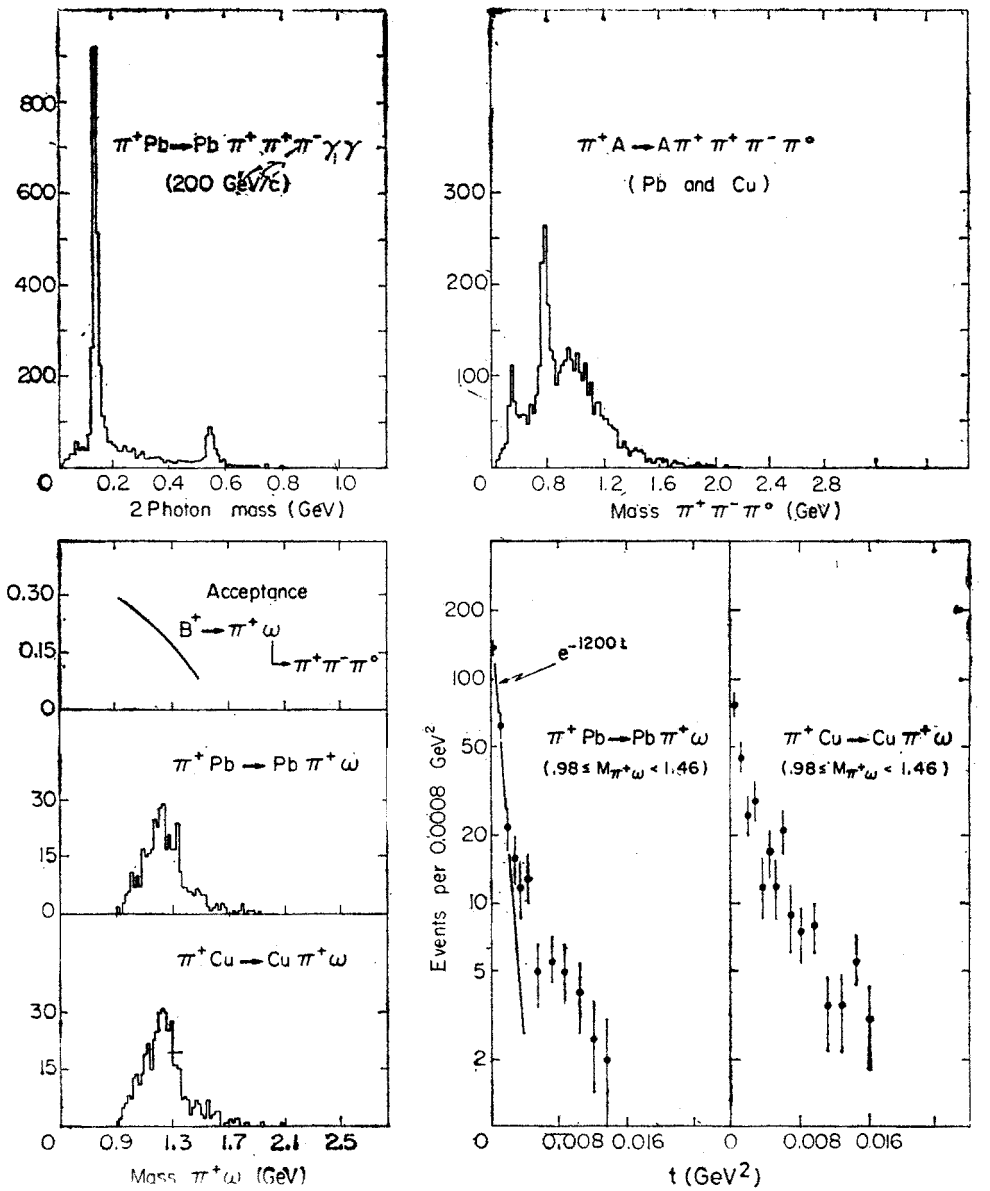

Fig. 17. Evidence for the electromagnetic production of the B(1235)$^+$ meson at 200 GeV/c

data is shown in Fig. 17. Again, the steep fall-off of the cross-section with increasing t[$\sim$ exp (1200 t) on Pb] can only be explained through the dominance of the Primakoff process in B production. We also observe a clear signal in both the $\pi^+\eta$ and $K^+K^0_s$ modes for A_2^+ production in the nuclear Coulomb field. Some of this evidence is presented in the mass spectra of Fig. 18. Table I summarizes our most recent measurements and compares these with simple quark-model predictions. In essence, it appears that the discrepancies

at the present time are rather small and these can probably be understood on the basis of anomalous (QCD) contributions to quark moments [20].

Except for the ρ^-, we have been first to clearly observe the radiative transitions of the states listed in Table I. Now that production in the nuclear Coulomb field has attained

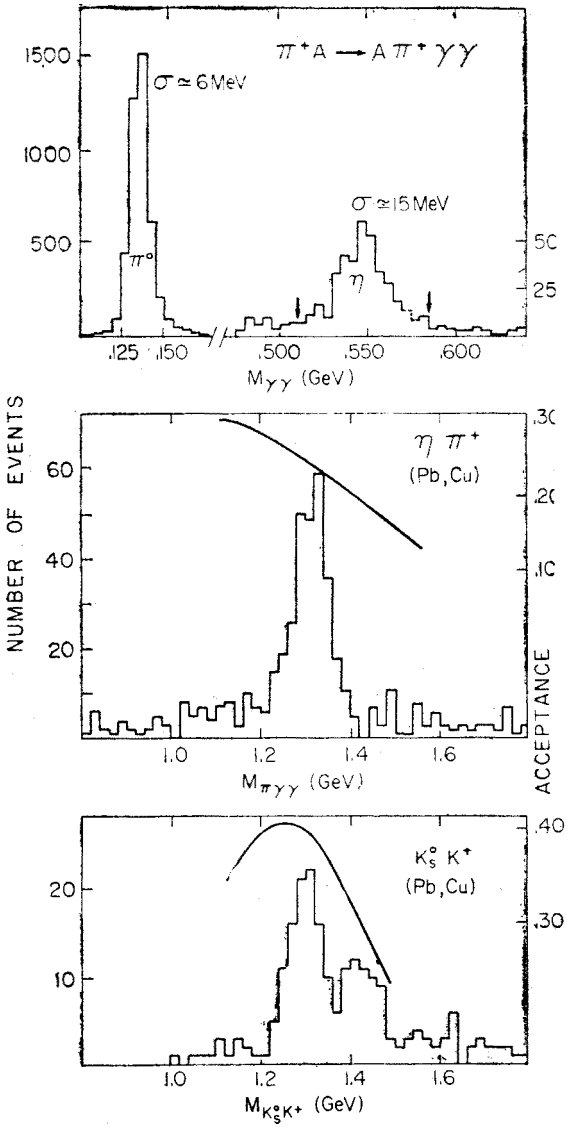

Fig. 18. Coherent production of A_2^+ mesons on nuclear targets at 200 GeV/c

maturity, we anticipate that, in the future, the study of $\pi\gamma$ and $K\gamma$ collisions will contribute not only to the elucidation of the properties of the known low-lying states but will also serve as a valuable exploratory tool in meson spectroscopy.

TABLE I

Summary of results from E272 — Radiative decays via Primakoff method

Transition[a]	Γ (keV)	Quark model[b] (keV)	
$\rho^- \to \pi^-\gamma$[c]	67 ± 7	85	
$K^{*-} \to K^-\gamma$[d]	62 ± 14	50	
$A_2^+ \to \pi^+\gamma$	300 ± 80	350	
$K^{*0+} \to K^+\gamma$	280 ± 80	310	
$B^+(1235) \to \pi^+\gamma$	Few hundred	100–500	Depends
$A_1^+ \to \pi^+\gamma$	Observed	300–3600	on S/D
$Q_A^+ \to K^+\gamma$	< 500	400–3900	ratio
Ratio	**Experiment**	**SU(3)**	**Broken SU(3)**
$\Gamma_{\omega\pi\gamma}/\Gamma_{\varrho\pi\gamma}$	11.8 ± 1.8	9	—
$\Gamma_{K^{*0}K^0\gamma}/\Gamma_{K^{*-}K^-\gamma}$	1.2 ± 0.7	4	1.6

[a] All but the ρ^- and K^{*-} rates are preliminary. [b] Babcock-Rosner, see Ref. [15]. [c] Ref. [12]. [d] Ref. [13]. [e] Ref. [16].

14. The production of direct photons at large p_T

The discovery [21] of the production of direct single photons in pp collisions at large transverse momenta had a highly stimulating effect on our group. We were fascinated by the possibility of studying the kinds of processes depicted in Fig. 19, and we were, of course, quite experienced in detecting photons. We decided that a serious investigation of single-photon production, using π^+, π^-, and proton beams, was not of great interest at present Fermilab energies, but quite the contrary for Tevatron energies. This is because QCD calculations become reliable only at large p_T, and a factor of two increase in incident momentum could increase yields by several orders of magnitude in the region of p_T ($\gtrsim 7$ GeV/c) where data might be interpretable in terms of the simple constituent-scattering graphs of Fig. 19. Consequently, our long-term programme was to study this proceess for 500–1000 GeV/c incident momenta and extract from the data the gluon structure functions of the incident hadrons and gluon fragmentation distributions. (The latter would be obtained by examining properties of hadronic jets recoiling from direct photons). But, because the cross-sections for direct-γ production are small and the backgrounds from π^0 and η^0 decays large, we felt it was necessary to do a test experiment prior to embarking on the Tevatron effort. We needed to know whether a LAC type of detector could be used in the kind of high interaction-rate ($\gtrsim 10^6$/s) environment that was required to challenge the small cross-sections. Also, we had to find out the detailed nature of the backgrounds we would have in such an experiment and how a LAC would function under such "battle" conditions. Could we extract a single-photon signal under the anticipated running conditions? Consequently, we proposed and executed a short test experiment (E629) to answer these questions and then to decide how to approach the experiment envisioned for the Tevatron stage [22].

Figure 20 shows a schematic diagram of the set-up for E629. The LAC was positioned with its centre about 1 m from the beam line. Special modules designed for the LAC output signals provided us with a global large-p_T trigger (p_T^{global}). This entailed forming a sum over all energies deposited in the individual channels in the front of the LAC, weighted

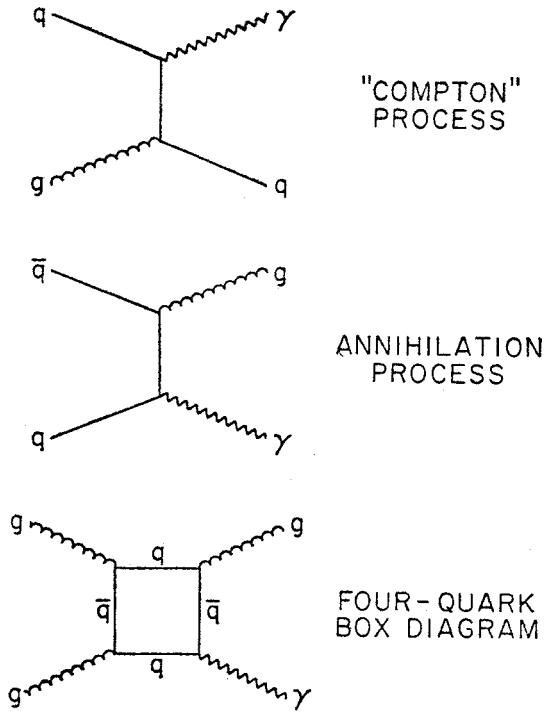

Fig. 19. Leading QCD graphs that contribute to the production of direct photons at large transverse momenta in hadronic collisions

(via a resistor chain) by the distance of any channel strip from beam centre. In addition, a local p_T requirement, over any three contiguous strips, of $p_T^{local} > {}^1/_3\, p_T^{global}$ was available for study. The latter was particularly valuable in suppressing triggers due to coherent noise (over the entire LAC) and due to contributions from events that had many low-$p_T\pi^0$ showers in the LAC.

Because of our interest in high data rates, we digitized, for off-line use, the times of arrival of the energy pulses in each of the channels in the front of the LAC. This information was invaluable for analysing our data. Another very important tool was the directionality of the LAC: the transverse position of an electromagnetic shower in the LAC can be measured to a precision of $\lesssim 1$ mm in the front and somewhat worse in the back. These two points along the direction of the shower cascade can be used to check whether the particle that initiated the shower originated from the target or from a different point in space.

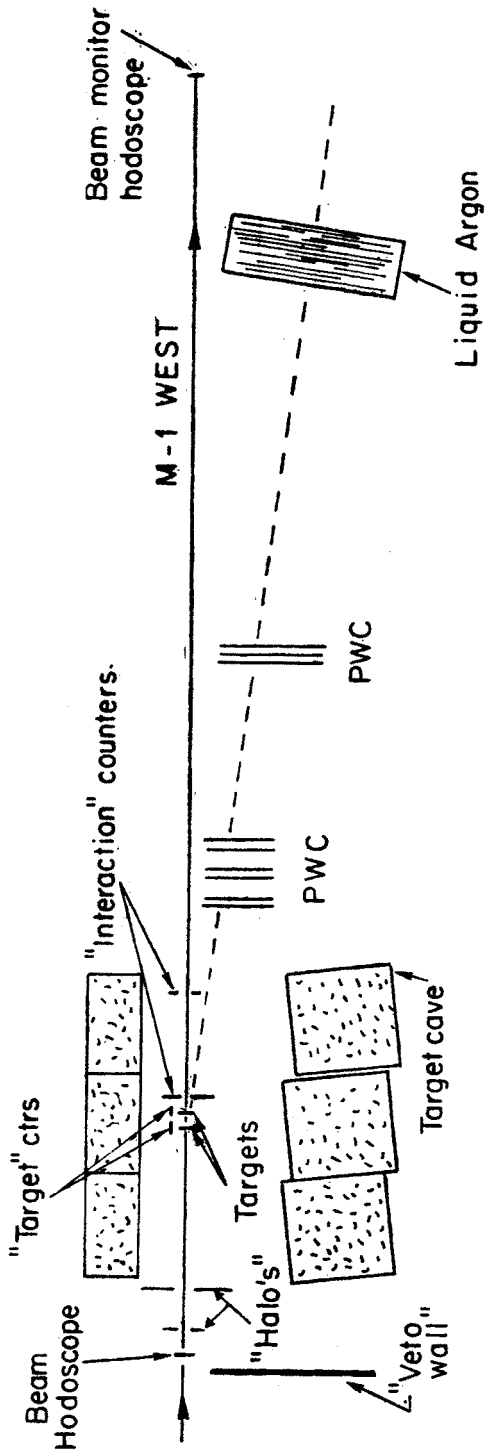

Fig. 20. Layout of equipment for experiment E629. This test was performed in a 200 GeV/c positive beam, utilizing nuclear targets of ~0.1 interaction lengths

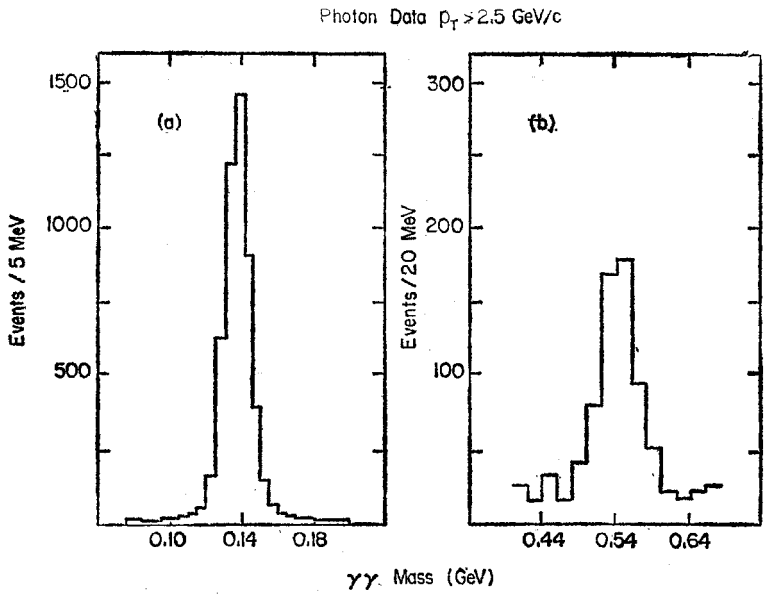

Fig. 21. The two-photon mass distribution for events that had only two reconstructed photons in the LAC

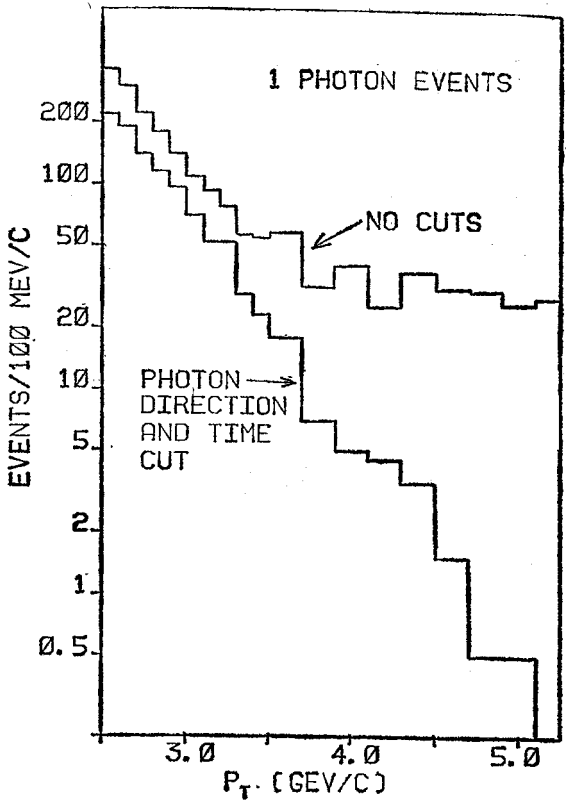

Fig. 22. The p_T distribution for single-photon events before and after timing and directionality cuts were applied to the showers

Figure 21 displays the two-photon mass distribution for $p_T > 2.5$ GeV/c, for triggers that contained only two reconstructed γ's in the LAC. Aside from the p_T cut-off on the two-photon systems, we demanded that the energies deposited in the LAC were within ± 20 ns of the expected time of arrival of the signals, and that the shower sum point to the target. The π^0 peak is essentially free of background, and the background at the η^0 mass is $\sim 10\%$ of the signal.

The p_T distribution observed for triggers on a carbon target that had single photons in the LAC is shown in Fig. 22. Requiring that the LAC signals are in time with the trigger counters and that the showers point to the target reduced the background level at large p_T by over an order of magnitude. (After the imposition of the directionality and timing cuts, the shape of the single-γ spectrum is very similar to that observed for the π^0 yield.)

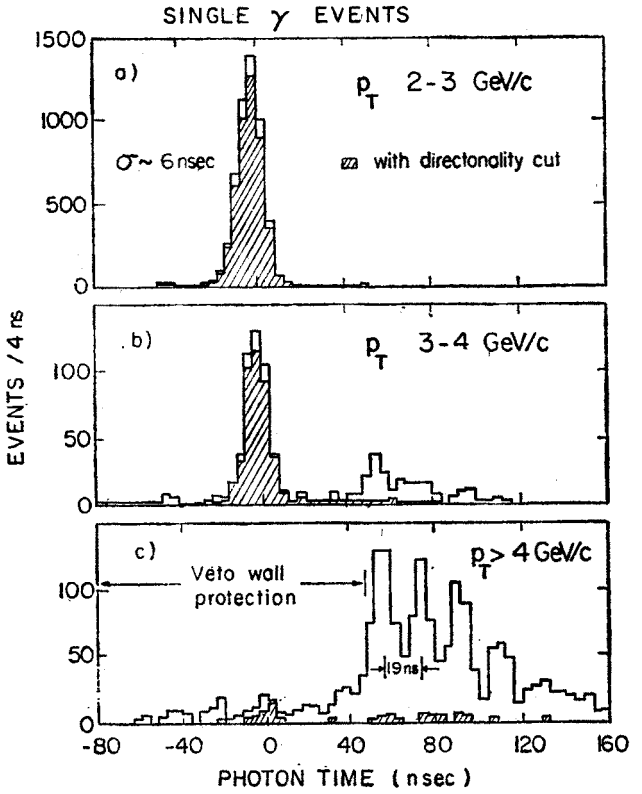

Fig. 23. The time of arrival of the energy pulses from the LAC, relative to the trigger counters ($t = 0$), as a function of the p_T of the single-γ

The times of arrival of the energy pulses for the single-shower data are shown in Fig. 23 as a function of the p_T of the shower. At low p_T's most of the events are in time and they point to the target (cross-hatched region). At higher p_T, as indicated in Fig. 22, most of the photons are out of time and do not point to the target. (In fact, the out-of-time showers,

which appear to display the ~19 ns RF structure of the accelerator beam, originate well upstream of the target region. Additional shielding placed upstream around the beam region would probably have drastically reduced this source of triggers.)

The observed γ/π^0 ratio for in-time events that point to the carbon target is shown in Fig. 24. The level of the single-γ signal at $\lesssim 3$ GeV/c is essentially what we expect from π^0 and η^0 background, and this background should fall somewhat with increasing p_T.

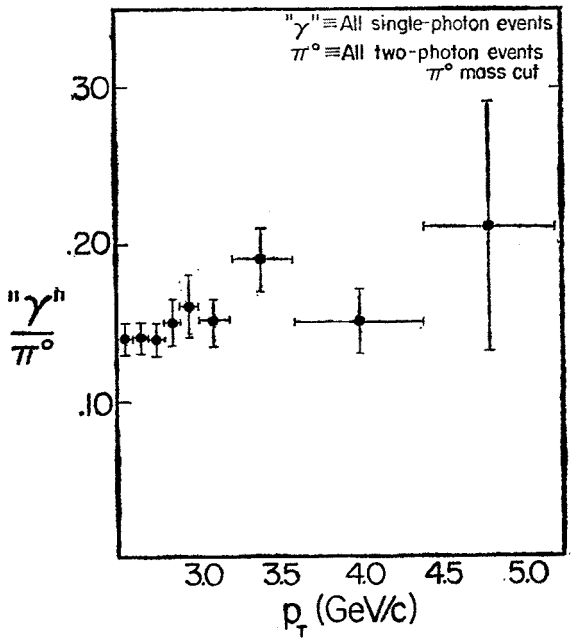

Fig. 24. The observed γ/π^0 ratio for single- and double-photon triggers

To conclude, we have observed a clean π^0 and η^0 signal under running conditions of ~10^6 interactions/s using a LAC. The decays of the π^0's and η^0's account for most, if not all, of the single-photon events. Thus, we believe that we have proved that the technique used in this test, namely, employing a LAC for measuring γ, π^0, and η^0 production at large p_T, is viable for use in a similar Tevatron experiment. We would have liked to have added methane to our LAC to see if the drift-time in the liquid argon would speed up by about a factor of 2–3, without causing excessive loss of pulse height, but our running priority was, unfortunately, not high enough at Fermilab for us to obtain the additional several days of beam time. (We did perform such a study in a small test calorimeter and got favourable results.)

The success of E629 prompted us to design and submit a more comprehensive experiment (E695) for the Tevatron stage. In Fig. 25 I display some of the special features of our proposed LAC that will undoubtedly provide us with the best photon detector at Fermilab (if the experiment is approved!).

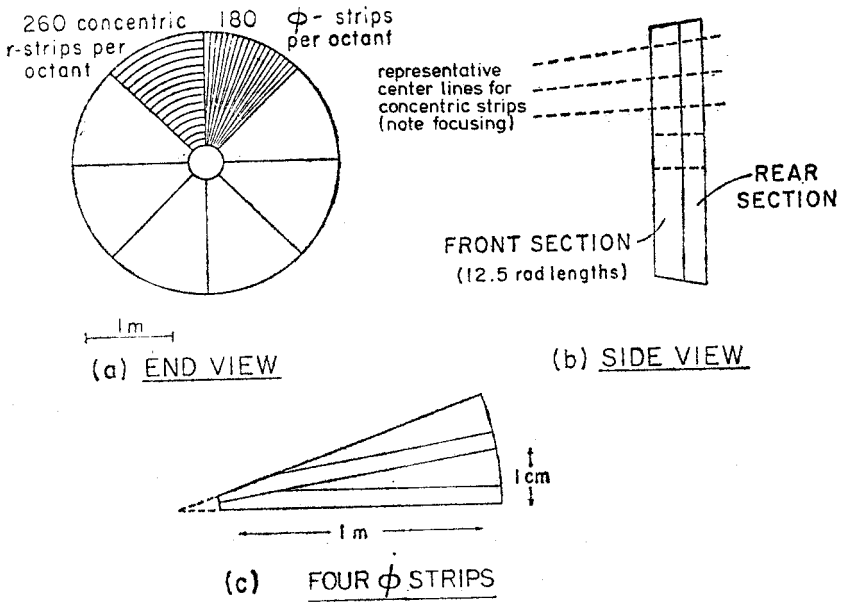

Fig. 25. Proposed design for LAC channels for E695

I thank Professors A. Białas, W. Czyż, W. Furmański, A. Kotański, K. Zalewski and their colleagues at the Krakow School for Theoretical Physics for providing me the pleasure of speaking at Paszkówka. I also wish to thank the Fabjan-Willis group for their hospitality during my stay at CERN and the EP Division for support. Finally, I thank my colleagues on E272 and E629 for their assistance in the preparation of the material for these lectures.

REFERENCES AND FOOTNOTES

[1] See, for example, Proc. First Workshop on Ultra-Relativistic Nuclear Collisions, ed. L. S. Schroeder LBL-8957 (1979).

[2] See G. Fäldt, *Nucl. Phys.* **B43**, 591 (1972) and references given therein to previous work.

[3] As I will mention shortly, the typical momentum transfers that are involved in the process are $\sim 10^{-5}$ GeV^2. Even for a carbon nucleus this corresponds to a transfer of ~ 1 keV of kinetic energy; this essentially guarantees that the nucleus remains in its ground state. I thank W. Czyż for a stimulating remark concerning this point.

[4] See, for example, J. Rosner, in *Techniques and Concepts of High Energy Physics*, ed. T. Ferbel, Plenum, New York 1981.

[5] See P. J. O'Donnell, in Proc. 16th Rencontre de Moriond 1981, ed. J. Tran Thann Van.

[6] B. Gobbi et al., *Phys. Rev. Lett.* **33**, 1450 (1974); *Phys. Rev. Lett.* **37**, 1439 (1976).

[7] A. N. Kamal, G. L. Kane, *Phys. Rev. Lett.* **43**, 551 (1979).

[8] The data served as the basis of a Ph. D. thesis on $\Gamma_{\varrho\pi\gamma}$ by T. Jensen (University of Rochester Report UR 747). I urge the reader to consult this work for additional detail on all aspects of E272. The following individuals participated in the experiment: D. Berg, J. Biel, C. Chandlee, S. Cihangir, B. Collick T. Droege, T. Ferbel, S. Heppelmann, J. Huston, T. Jensen, A. Jonckheere, T. Joyce, P. Koehler,

F. Lobkowicz, Y. Makdisi, M. Marshak, M. McLaughlin, C. Nelson, T. Ohshima, E. Peterson, K. Ruddick, M. Shupe, P. Slattery and P. Thompson (Fermilab-Minnesota-Rochester Collaboration).

[9] T. Droege, F. Lobkowicz, Y. Fukushima, Fermilab Report TM-746 (Oct. 1977).

[10] C. R. Kerns, Fermilab Report TM-819 (Oct. 1978).

[11] P. Feller et al., *Nucl. Phys.* **B104**, 219 (1976).

[12] For more details see Ref. [8] and D. Berg et al., *Phys. Rev. Lett.* **44**, 706 (1980); also a *Phys. Rev.* article (in preparation).

[13] D. Berg et al., *Phys. Lett.* **98B**, 119 (1981).

[14] C. Bemporad et al., *Nucl. Phys.* **B51**, 1 (1973).

[15] See Eq. (2) and, for example, J. Babcock, J. Rosner, *Phys. Rev.* **D14**, 1286 (1976).

[16] W. Carithers et al., *Phys. Rev. Lett.* **35**, 349 (1975).

[17] G. L. Greene et al., *Phys. Rev.* **D20**, 2139 (1979); L. Schachinger et al., *Phys. Rev. Lett.* **41**,1348 (1978).

[18] A. Jonckheere et al., *Nucl. Instrum. Methods* **180**, 25 (1981).

[19] See reference given in footnote [15].

[20] See, for example, D. Geffen, W. Wilson, *Phys. Rev. Lett.* **44**, 370 (1980).

[21] See, for example, M. Diakonou et al., *Phys. Lett.* **91B**, 301 (1980), and references given therein to previous work.

[22] The collaborators on E629/E695 include: J. Biel, T. Droege, A. Jonckheere, P. Koehler and C. A. Nelson, Jr., (Fermilab), C. Bromberg, S. Cooper, R. A. Lewis, R. Miller, B. Y. Oh, G. A. Smith and J. Whitmore (Michigan State University), K. Heller, M. Marshak, E. Peterson, J. Povlis, K. Ruddick and M. Shupe (University of Minnesota), B. Brown, D. Garelick, G. Glass, M. Glaubman, J. Pothier and Han Shu-Rong (Northeastern University), C. Chandlee, S. Cihangir, T. Ferbel, J. Huston, J. LeBritton, F. Lobkowicz, M. McLaughlin, P. Slattery and M. Zieliński (University of Rochester).